CFD computations of wind turbine blade loads during standstill operation KNOW-BLADE, Task 3.1 report

Sørensen, Niels N.; Johansen, Jeppe; Conway, S.

Publication date:
2004

Document Version
Publisher's PDF, also known as Version of record

Risø-R-1465(EN)

CFD Computations of Wind Turbine Blade Loads During Standstill Operation KNOW-BLADE TASK 3.1 Report

N. N. Sørensen, J. Johansen, S. Conway

Risø National Laboratory, Roskilde, Denmark
June 2004

Abstract Two rotors blades are computed during standstill conditions, using two different Navier-Stokes solvers EDGE and EllipSys3D. Both steady and transient linear $k-\omega$ RANS turbulence models are applied, along with steady non-linear RANS and transient DES simulations. The STORK 5.0 WPX blade is computed a three different tip pitch angles, 0, 26 and 50 degrees tip pitch angle, while the NREL Phase-VI blade is computed at 90 degrees tip pitch angle. Generally the CFD codes reproduce the measured trends quite well and the two involved CFD codes give very similar results. The discrepancies observed can be explained by the difference in the applied turbulence models and the fact that the results from one of the solvers are presented as instantaneous values instead of averaged values. The comparison of steady and transient RANS results show that the gain of using time true computations are very limited for this case, with respect to mean quantities. The same can be said for the RANS/DES comparison performed for the NREL rotor, even though the DES computation shows improved agreement at the tip and root sections. Finally, it is shown that the DES methodology provides a much more physical representation of the heavily stalled part of the flow over blades at high angles of attack.

ISBN 87-550-3343-1(internet)
ISSN 0106-2840

Contents

1 Introduction

One of the important load cases, when designing a wind turbine, is the case of rotor standstill at high wind speeds. Little effort has been put into investigating the actual load distribution for this case and very few detailed measurements exist. Normally, when working with typical aeroelastic design codes, computations for these situations are based on the Blade Element Momentum or lifting line methods, both relying on tables of airfoil lift and drag. As very little data exist for airfoils at very high angles of attack (above 40 degrees) and knowledge of eventual 3D effects are limited, these computations become very uncertain. The present work is aimed at improving the knowledge about rotor standstill by analyzing the problem using Computation Fluid Dynamics on parked wind turbine blades.

Investigation of loads during parked conditions, was done by other authors, Ostowari et al. [5] and [6] investigated untwisted blades with NACA 44XX airfoils, Dahlberg et al. [15] investigated parking loads on a 2.4 meter wind turbine blade in a wind tunnel, and the recent large scale experiment by NREL also includes parked loads, see Simms [8]. Several investigation were performed on turbine blades in the atmosphere, Dekker et al. [18], Paulsen [27] and Brand et al. [1]. Several authors suggest formulas for computing the drag distribution, Dahlberg et al. [15], Montgomerie [2] and Lindenburg [4]. The main problem of estimating the spanwise drag distribution is that in most of the investigations, only load measurements are available, either flapwise bending moments or thrust coefficients, leaving a great deal of uncertainty about the actual distribution.

Previously, Navier-Stokes solvers were applied to airfoils at high angles of attack Yang et al. [30], resulting in heavily overprediction of the loads. This is in good agreement with the general findings when applying Navier-Stokes solvers to stalled airfoils, where predictions slightly above the stalling angle are know to result in too high lift, Bertagnolio [9]. The main mechanisms behind this shortcoming is believed to be suppression of the 3D breakup of the flow in the separated area, supporting artificially large separation bubbles, Johansen et al. [14].

In parallel to the present investigation, an investigation was carried out in a National Danish Research program, were it was demonstrated that CFD predictions show very good agreement with measurements for flat plates at 90 degrees angle of attack, a situation with some similarities to the parked wind turbine blade, see [24]. Following this validation, the code was applied to a series of wind turbine blades, the LM8.2, LM19.1 and a modern blade intended for use on a MW turbine.

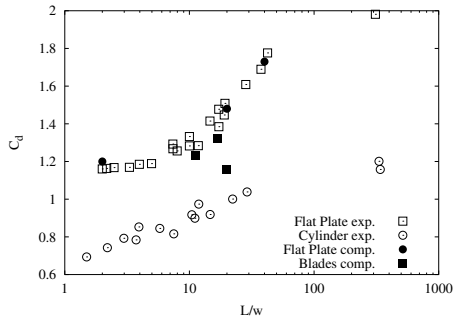

Figure 1. Comparison of computed drag for flat plates and blades with measured values for flat lates and cylinders.

In the present investigation two different CFD codes, one compressible and one incompressible, was applied to two different rotor geometries, namely the NREL

Phase-VI rotor at 90 degrees tip pitch and the Swedish STORK 5.0 WPX rotor at 0, 26 and 50 degrees tip pitch. The computations were compared to measured pressure distributions and integrated forces on the rotor blades. Additionally, the spanwise force distributions was extracted from the computations.

2 Method

The flow solution around the parked rotors are computed by two different flow solvers, namely the Swedish Edge code and the Danish EllipSys3D code.

2.1 Navier-Stokes Solvers

The Risœ/DTU EllipSys3D code is developed in co-operation between the Department of Mechanical Engineering at DTU and The Department of Wind Energy at Risø National Laboratory, see Michelsen[16, 17] and Sørensen[23]. The EllipSys3D code is a multiblock finite volume discretization of the incompressible Reynolds Averaged Navier-Stokes (RANS) equations in general curvilinear coordinates. As the code solves the incompressible flow equations, no equation of state exists for the pressure, and the PISO algorithm of Issa [12], [13] is used to enforce the pressure/velocity coupling. The solution of the Poisson system arising from the pressure correction equation is accelerated using a multigrid method. The solution is advanced in time using a 2nd order iterative time-stepping (or dual time-stepping) method. In each global time-step the equations are solved in an iterative manner, using underrelaxation. The convective terms are discretized using a third order upwind scheme, implemented using the deferred correction approach first suggested by Khosla and Rubine [19]. Central differences are used for the viscous terms. In each sub-iteration only the normal terms are treated fully implicit, while the terms from non-orthogonality and the variable viscosity terms are treated explicitly. In the present work the turbulence in the boundary layer is modeled by the k-ω SST eddy viscosity model of Menter [28] for the RANS simulations, while the Detached Eddy Simulation model of Strelets [22] is used for the DES simultations. The EllipSys3D code is parallelized with MPI for execution on distributed memory machines, using a non-overlapping domain decomposition technique.

The FOI EDGE solver, is a flow solver for unstructured grids of arbitrary elements, see [25]. Edge solves the Reynolds Averaged Navier-Stokes compressible equations in either a steady frame of reference or in a frame with system rotation. Turbulence can be modelled with differential eddy viscosity models or explicit algebraic Reynolds stress models. The solver is based on an edge-based formulation and uses a node-centered finite-volume technique to solve the governing equations. The control volumes are non-overlapping and are formed by a dual grid obtained from the control surfaces for each edge. All elements are connected through matching faces. The governing equations are integrated explicitly towards steady state with Runge- Kutta time integration. The convergence is accelerated with agglomeration multigrid and implicit residual smoothing. EDGE contains different spatial discretizations for the mean flow as well as the turbulence, different gas models, steady state and time accurate time integration, low speed preconditioning etc. The turbulence in the boundary layer is modeled by the original k-ω eddy viscosity model of Wilcox [7], and the Wallin and Johansson explicit Algebraic Stress Model based on the Wilcox k-ω model [29]. For the present compuations the central difference scheme with artificial dissipation is used for the convective terms.

3 Geometry and computational mesh

In the present investigation two different rotor blade geometries are investigated during standstill, namely a blade from the NREL Phase-VI rotor and the Swedish STORK 5.0 WPX wind turbine blade. The surface geometries and the mesh generation process is described below.

The NREL PHASE-VI rotor is a tapered and twisted rotor blade based on the S809 airfoil with a span of 5 meters, for more details on the actual blade layout see [26]. The STORK 5.0 WPX blade is based on the NACA-4412 airfoil, the blade has a span length of 2.375 meters and has both taper and twist, for more details on the blade layout see [11].

3.1 Surface generation

For the main part of the blade the geometry is described by the 2D airfoil geometries. For the NREL PHASE-VI rotor the theoretical coordinates of the S809 airfoil is used. For the STORK rotor measured cross sections at eight spanwise sections are used, due to the high deviation from the theoretical values reported in [11]. For the NREL PHASE-VI the tip geometry is based on digitized geometry kindly provided by E.P.N. Duque Northern Arizona University. The tip geometry of the STORK blade is based on the information provided in [11].

For the main part of the blades in-house Risø software is used to construct a surface mesh based on a spline representation of the sectional information, while the outermost 5 % of the blade near the tip, where the surface is strongly double curved either, the MEGACADS program by DLR or in-house hyperbolic surface-mesh generator are used. The surface meshes have 256 cells in the chordwise direction, and respectively 64 cells for the STORK blade, and 256 cells for the PHASE-VI blade in the spanwise direction. The tip geometry is resolved using a 'box-topology' placing an extra block of 64×64 cells right at the tip, see Figur 2.

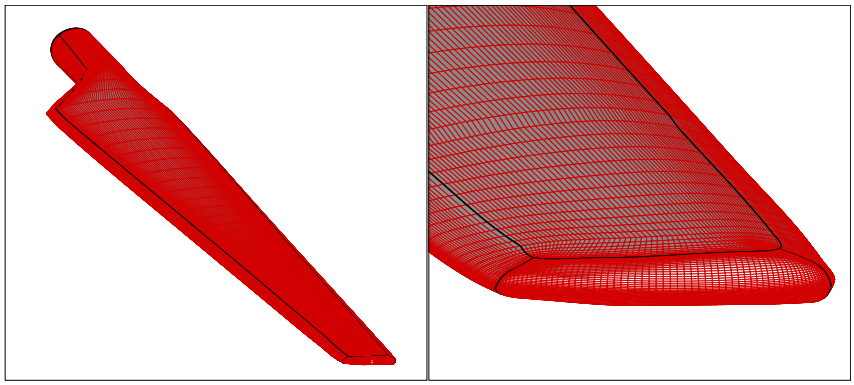

Figure 2. The surface mesh used for the STORK 5.0 WPX blade. The block topology at the blade tip can be seen in the right picture.

3.2 Volume Mesh Generation

The volume mesh around the blades are constructed in the following way. Based on the surface mesh, an O-O-mesh is constructed around the blade using the Risø

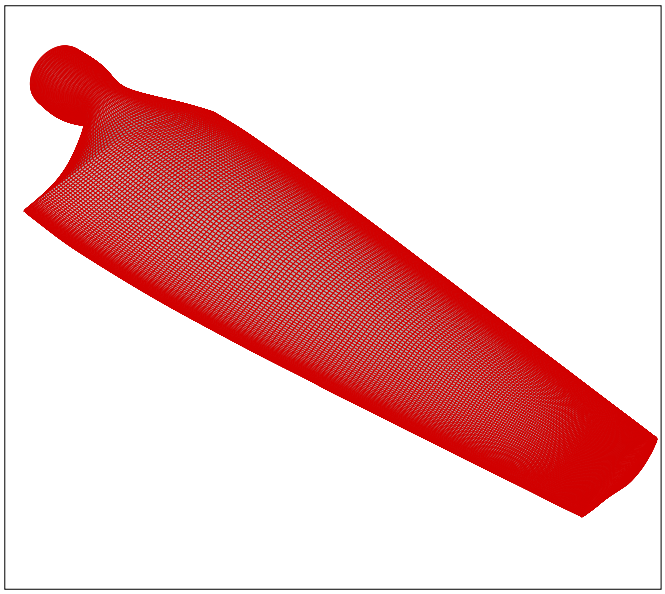

Figure 3. The surface mesh used for the NREL PHASE-VI computations, the high spanwise density, necessary for the DES computations, is very different from the spanwise resolution used for the STORK blade.

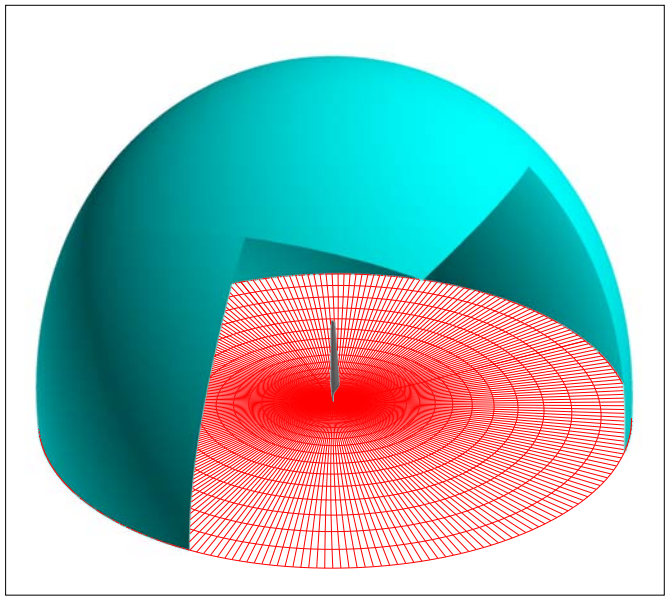

Figure 4. Picture of the mesh used for the STORK 5.0 WPX computation, showing the location of the outer boundary, the symmetry plane and the blade surface.

HypGrid3D hyperbolic mesh generation code. The external boundary of the outer O-topology is nearly spherical and placed approximately 2.5 to 3 blade lengths away from the blade surface. The normal cell size at the wall is set to $y^+ \sim 2$ to resolve the boundary layer, the points in the normal direction are distributed using a hyperbolic tangent function. For the STORK rotor 64 cells are used in the normal direction, while 128 cells are used for the PHASE-VI blade. For the PHASE-VI blade, the normal distribution is specifically controlled to assure nearly cubic cells in an area close to the blade surface. The mesh for the STORK computations

consists of 1.3 million cells, while the NREL PHASE-VI mesh has 8.9 million points.

The location of the inlet and outlet boundary conditions can be seen in Figur 4, where the blade is visible through the outlet section, while inflow conditions are specified over the remaining part of the outer dome. A no-slip conditions is used on the blade surface, and a symmetry conditions is used at the bottom plane.

4 Results

This section presents comparisons of the computed and measured results for the STORK rotor involving several different types of RANS computations. This is followed by RANS and DES results for the NREL PHASE-VI rotor compared with measurements.

4.1 STORK Rotor Blade

The computed cases for the STORK rotor blade are listed in Table 1. The cases are chosen so that there is one fully attached case, one partially stalled and one fully stalled case. More details about the measurements can be found in [10, 3], where both the instrumentation and the tunnel facility are described in detail. During the measurement campaign the pressure was measured at eight spanwise locations with several of the stations placed close to the tip, r/R=[0.30, 0.55, 0.75, 0.85, 0.925, 0.95, 0.975, 0.99].

As previously mentioned two different Navier-Stokes solvers are applied to the STORK rotor blade computations, the computations performed by Risø using the EllipSys3D code are both computed as steady state and time true solutions, while all computations performed by FOI, using the EDGE code, are steady state. The time true solutions are all computed using a time step of $1.\times10^{-4}$ sec. Additionally, the original version of the $k-\omega$ model, used in the FOI computations, for both the EARSM and the pure $k-\omega$ simulations, are known to under-predict the amount of separation compared to both measurements and the SST version used by Risø. It is important to remember these differences when comparing the results, as both will lead to differences between the two sets of computations. To minimize the differences, both codes uses the same computational mesh.

Table 1. Operational condition for the STORK compuations.

CASE	Wind Speed [m/s]	Tip Pitch [deg.]	Pressure [Pa]
1	14.72	0.00	138.2
20	15.09	26.00	129.9
28	15.08	50.01	139.4

The computed values for the flap, pitch and edge wise moments around the rotor centre, for the three cases are listed in Table 2. Comparing the unsteady and the steady computations, we observe that there is very little difference.The Risø computations show, a maximum deviation of 2.8% on the flap-wise bending moment in case-28 while the edge-wise moment shows a deviation of 8.3%. Comparing the FOI and the Risø results, there is very good agreement for the pitch moment, while the predictions of the edge-wise moments show large deviations. Looking at the flap-wise bending moment, the difference is around from 5 % to 15 %. For the Risø computations the loads have been averaged over several iterations or timesteps, whereas the FOI results are shown for the final iteration, irrespectively a steady state solution may not be obtained. Looking at the iteration/time traces of the Risø computations, not shown here, the variation around the mean value will generally not explain the difference. The deviations are believed to be caused mainly by the difference in the applied turbulence models.

Looking into more details, the spanwise distributions of the tangential forces (F_x) and the flap-wise forces (F_z)are compared, see Figur 5 to 7. Since only the pressure distributions are available from measurements, the measured values

Table 2. Flap, pitch and edge-wise moment for the three cases.

CASE	Component	FOI STEADY	RISOE STEADY	RISOE UNSTEADY
1	Flap	-3.6	-3.8	
	Pitch	-1.3	-1.3	
	Edge	-3.6	-2.8	
20	Flap	97.3	85.0	83.0
	Pitch	-1.0	-0.9	-0.9
	Edge	14.7	9.0	9.3
28	Flap	103.6	108.0	105.0
	Pitch	-2.5	-2.4	-2.4
	Edge	6.8	6.5	6.0

shown in these figures are based solely on pressure, neglecting the contribution from skin-friction. Generally, the spanwise force distributions computed by FOI and Risø show overall good agreement, especially if we remember that the FOI forces are based on snap-shots while the Risø forces are averaged over several iterations. For the 50 degree angle of attack, case-28, the FOI forces exhibits large spanwise fluctuations, which is definitely caused by the lack of averaging.

Looking in details at Figur 5, the computations and the measurements show the same trends with a negative tangential force, and the same monotone increasing spanwise force with radius. Looking at the corresponding pressure distributions, Figur 8, the overall shape of the pressure distributions are in good agreement with the measured values both for the FOI and the Risø computations. But, since the forces shown in Figur 5 are a result of the sum of two areas with opposite sign, the agreement is hard to judge visually. The facts that the Reynolds number is low and the angle of attack around 6 degrees, make it difficult to predict the flow correctly using a fully turbulent assumption.

As the angle of attack is increased, the relative error between the computed and measured values decreases, and the agreement between the measured and computed edge-wise and flap-wise forces are generally good, see Figur 6. Compared to case-01, most of the spanwise stations are well within the fully separated region, and the influence of the Reynolds number has vanished. Generally, the FOI predictions show higher edge and flap forces, due to the lesser tendency towards stall for the original $k-\omega$ model used in the EDGE predictions. This is a direct reflection of the pressure distributions, most clearly seen for case-20, see Figur 9, where the original $k-\omega$ model fails to capture the correct stall of the airfoil along the total blade span. The SST version of the $k-\omega$ model used in the Risø computations also fails to predict the correct stalling behaviour, but only for the 55 % section, while the remaining sections are predicted with good accuracy.

For the highest tip pitch angles, case-28, there is good agreement between the computed and measured forces. For the FOI force distributions spanwise variations are seen, that may originate from the lack of averaging. This behaviour is also seen for the pressure distributions, Figur 10. The pressure distributions computed by Risø show excellent agreement with the measured values, which is also reflected in the force distributions, see Figur 7.

For case-01 where both the original $k-\omega$ model and the EARSM model are applied by FOI, only small differences are observed indicating that the use of the Reynolds Stress model does not change the flow considerably. Looking at case-28, it is difficult to derive the influence of the EARSM model, as the pressure contours show 'unsteady' behaviour because of lack of convergence.

Finally, the computed skin-fricition distributions are shown in Figurs 11 to 13 for future reference. As no measurements exist for this quantity we will not discuss this in detaill, but only state that the agreement between the FOI and RISOE results are generally good for this quantity.

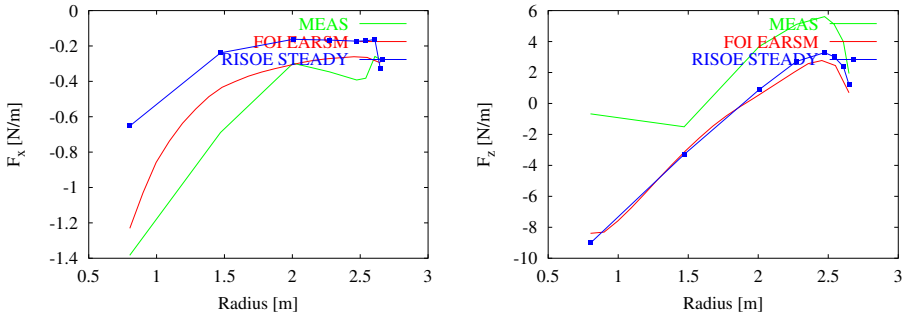

Figure 5. Spanwise distribution of the tangential and axial force components for CASE-01

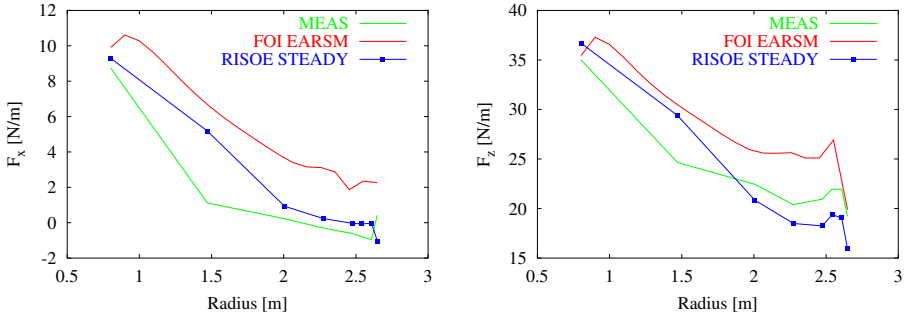

Figure 6. Spanwise distribution of the tangential and axial force components for CASE-20

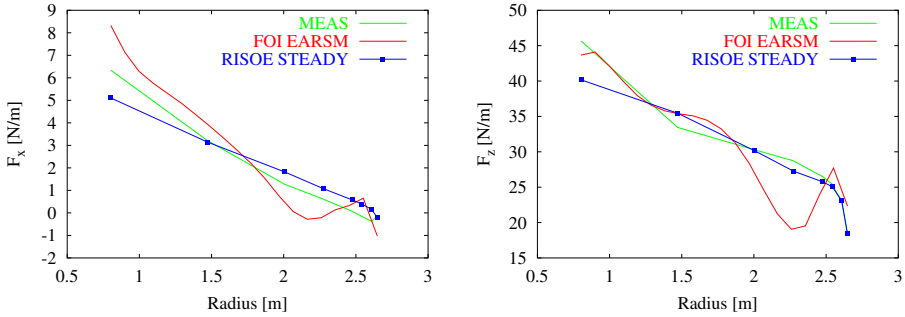

Figure 7. Spanwise distribution of the tangential and axial force components for CASE-28

Overall performance of the STORK computations

The computations revealed very limited difference between steady state and time true computations for the cases. Based on this, we may conclude for time averaged

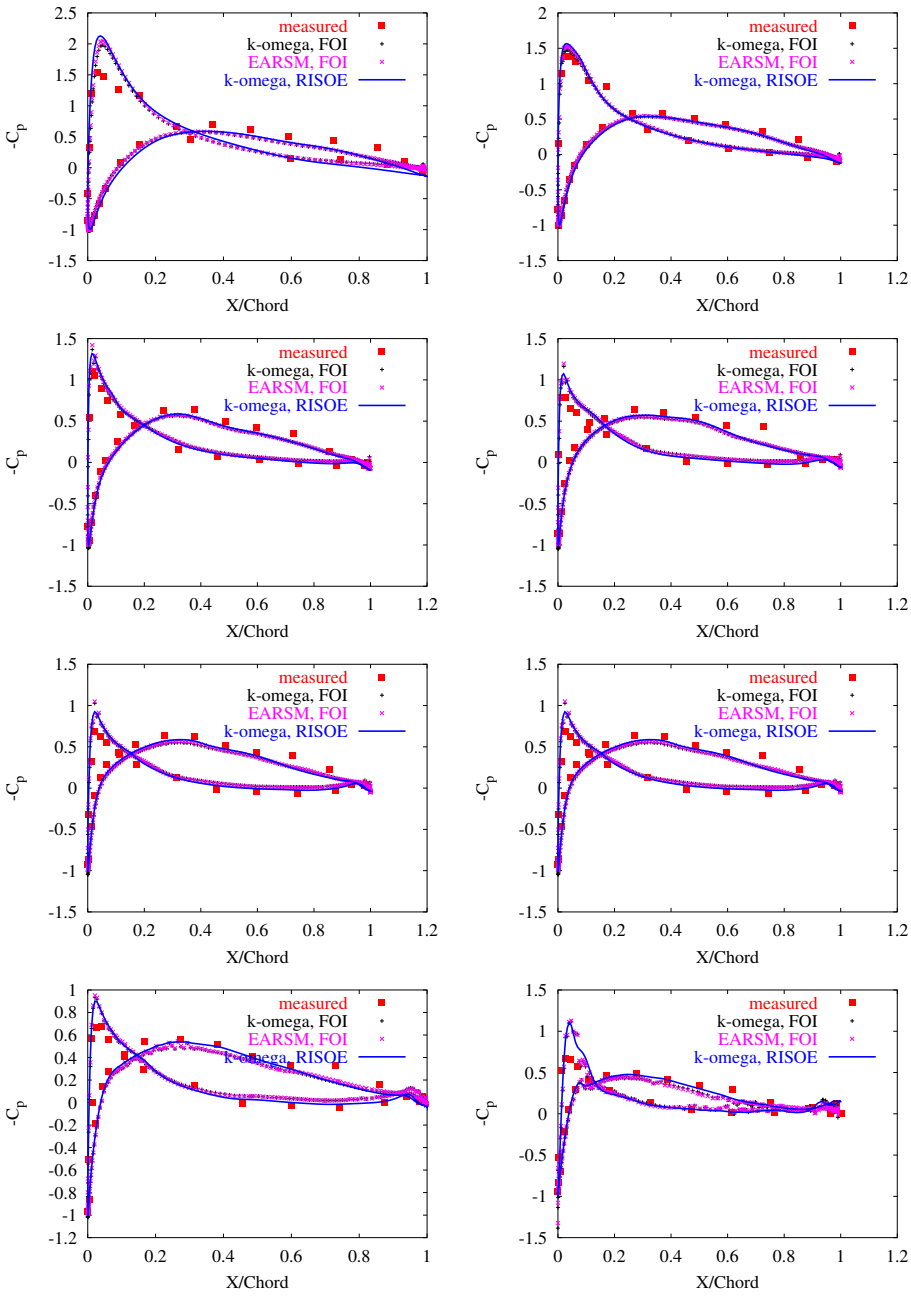

Figure 8. Comparison of the computed and measured pressure distributions for CASE-01.

values, transient computations with the time steps used in the present investigation do not offer any advantages compared to steady state computations. The effect of the non-linear $k-\omega$ model used for case-28 is difficult to evaluate, as the results presented are obscured by the fact that the results are instantaneous values. Except for the lowest angle of attack, case-01, the agreement with the measured value are generally good. Especially at the highest tip pitch angle, case-28, the agreement is very good. The comparison of the pressure curves verifies the well known superiority of the SST $k-\omega$ model over the original $k-\omega$ model for airfoil flows.

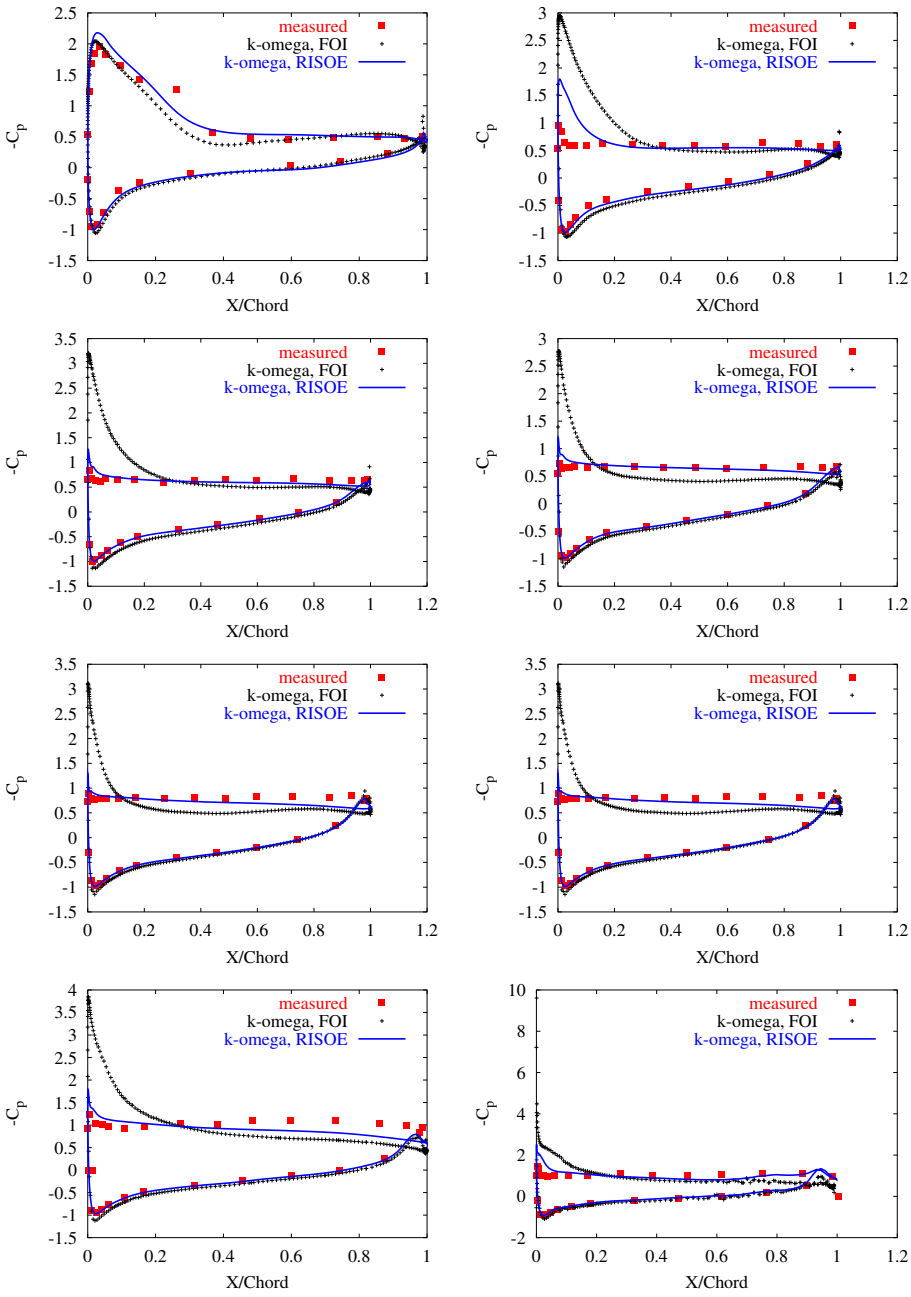

Figure 9. Comparison of computed and measured pressure distributions for CASE-20.

4.2 NREL PHASE-VI blade

For the NREL Phase-VI rotor only a single configuration is computed, namely the case where the flow is 90 degrees to the tip chord. The case is named L2000ST0 and the operational conditions are given in Table 3. Risø has performed two computations using the EllipSys3D code, one using the SST $k-\omega$ model in its standard Reynolds Averaged version, and one using the Detached Eddy Simulation version of the same model. The computational mesh, the time step, the differencing scheme, etc. are the same for the two computations i.e, only the turbulence model is changed.

During the measuring campaign, [20] and [21] pressure distributions where

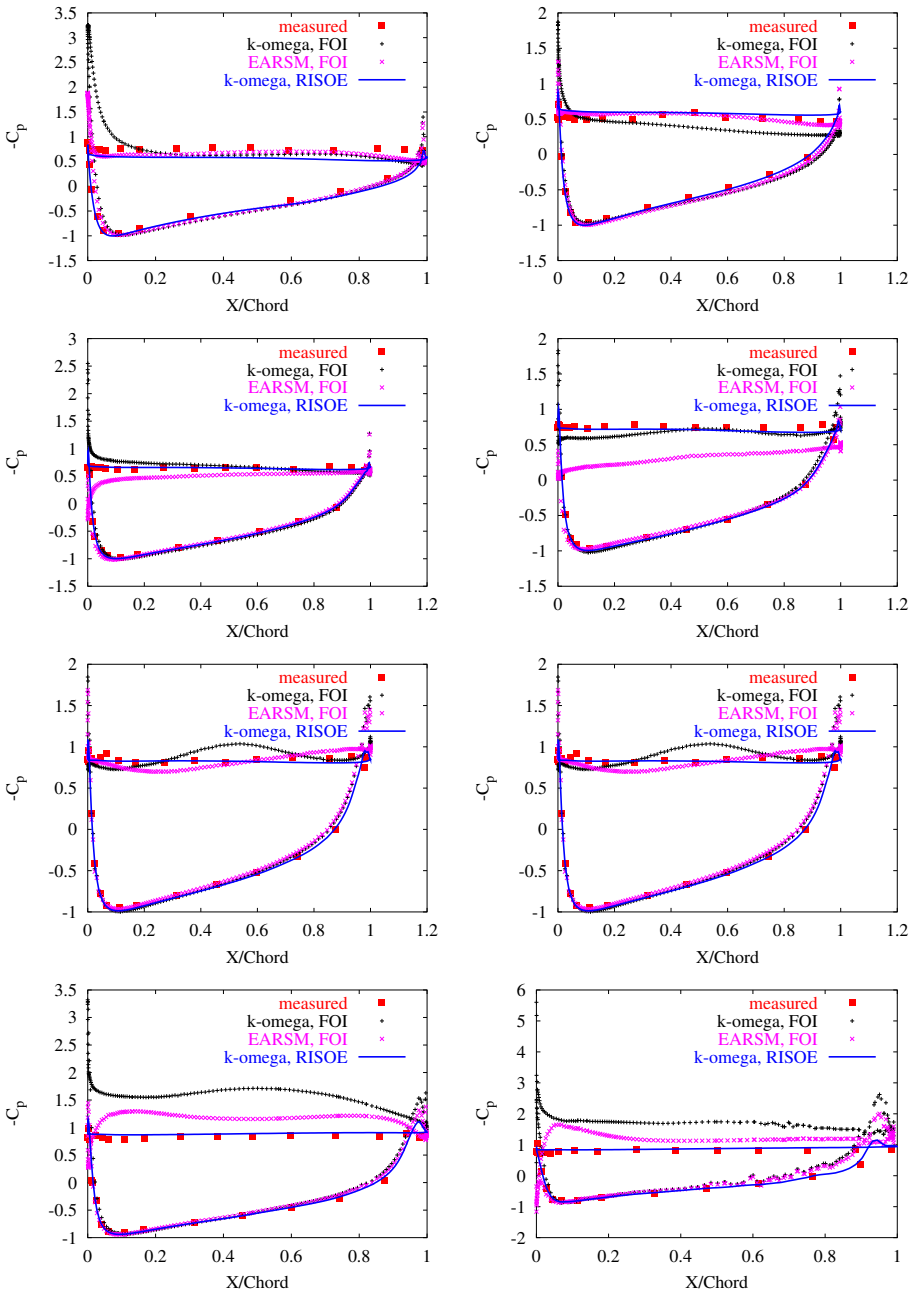

Figure 10. Comparison of computed and measured pressure distributions for CASE-28

measured at r/R=[0.30, .47, .63, .80, .95] along with moments at the blade shaft. Additionally, time series of the sectional force components are available in the previous mentioned five radial stations, along with time averaged values.

Table 3. Operational condition for the NREL PHASE-VI parked compuations.

CASE	Wind Speed [m/s]	AOA of Tip [deg.]	Density $[kg/m^{-3}]$	Viscosity $\times 10^5$
L2000ST0	20.0	90.00	1.2318	17.7875d-6

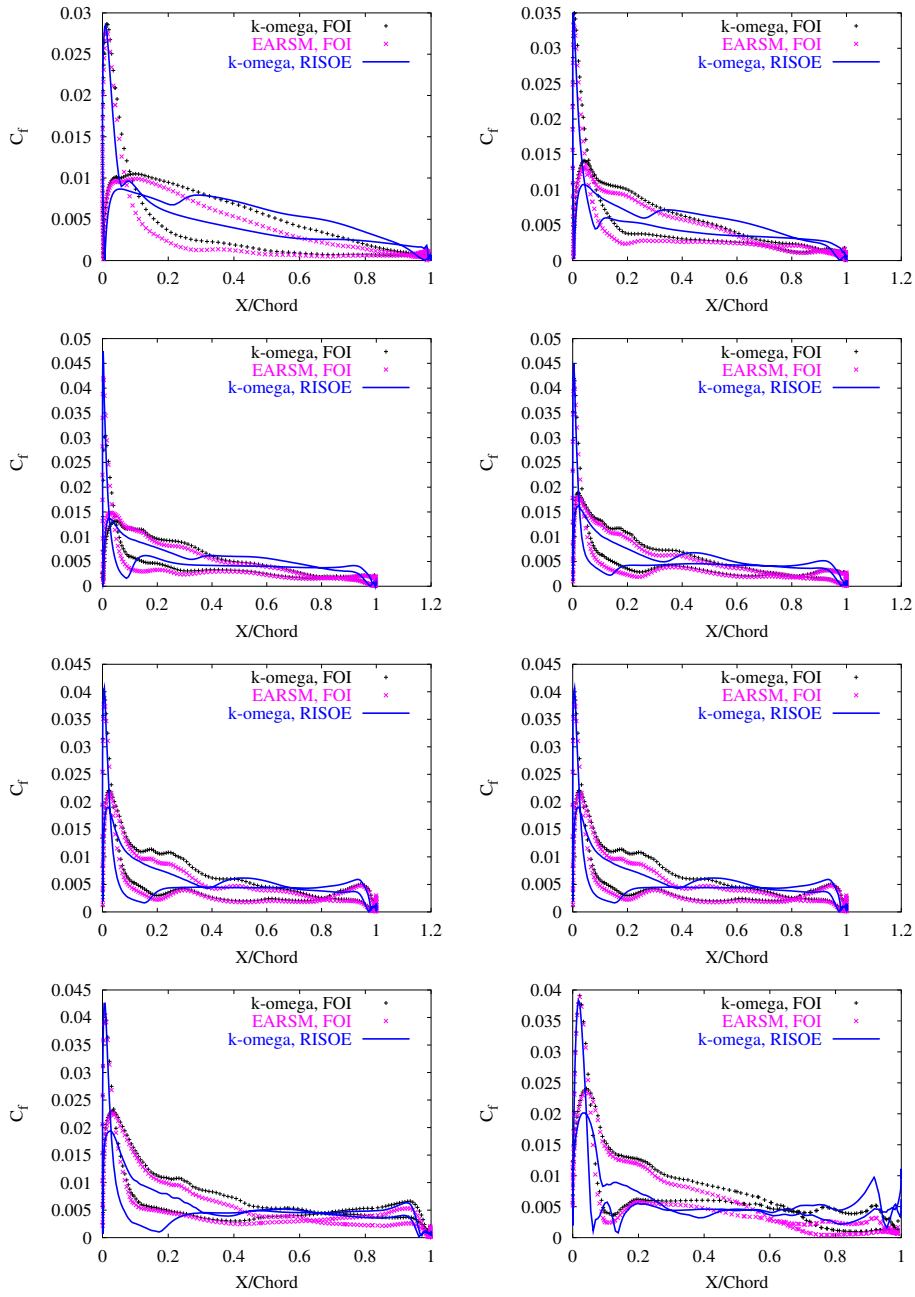

Figure 11. Comparison of the computed skin friction distributions for CASE-01.

Comparing the blade root flap and edge moments at r=0.432 [m], see Table 4, good agreement is observed with a maximum deviation of around 8 percent for the edge moment in the RANS simulation. For the flap wise bending moment the errors of both simulations are below 1 percent.

The spanwise distribution of the tangential and normal force coefficients along the blade span are shown in Figure 14. The figures shows that the difference between the mean values of the DES simulation and the RANS simulation are very small, indicating limited gain by running the DES simulation with respect to these time averaged quantities. Comparing with the measured data, the deviation along the major part of the blade is around 20% for the normal force coefficient while the tangential force coefficient deviates around 10-15%, Figure 14. Looking

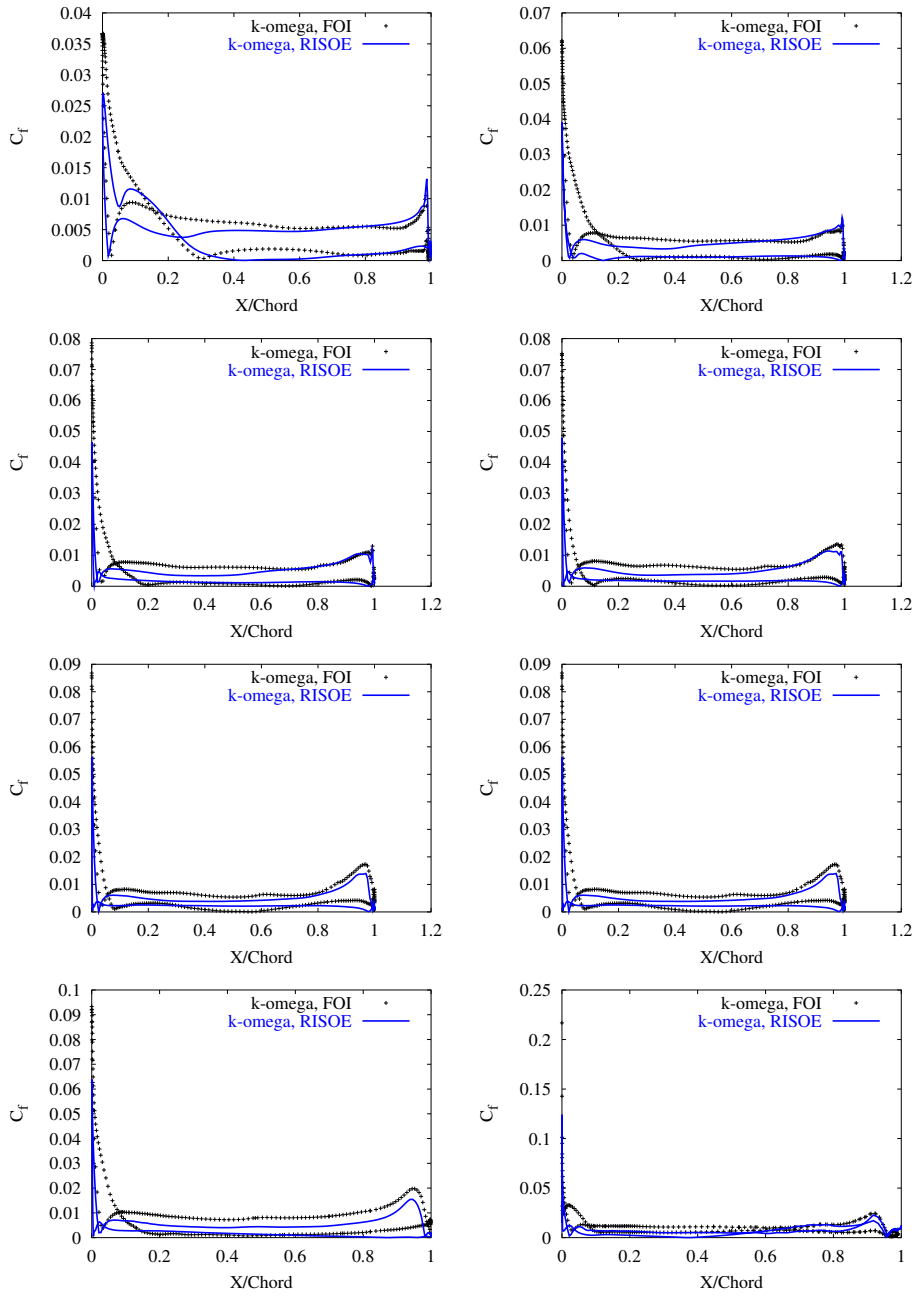

Figure 12. Comparison of the computed skin friction distributions for CASE-20.

at the pressure distributions along the blade span, we see that the overestimation of the normal coefficient is caused by overprediction of suction on the lee side of the profiles. Looking at the upstream side of the blade, the pressure distributions agree excellent agreement, Figure 15.

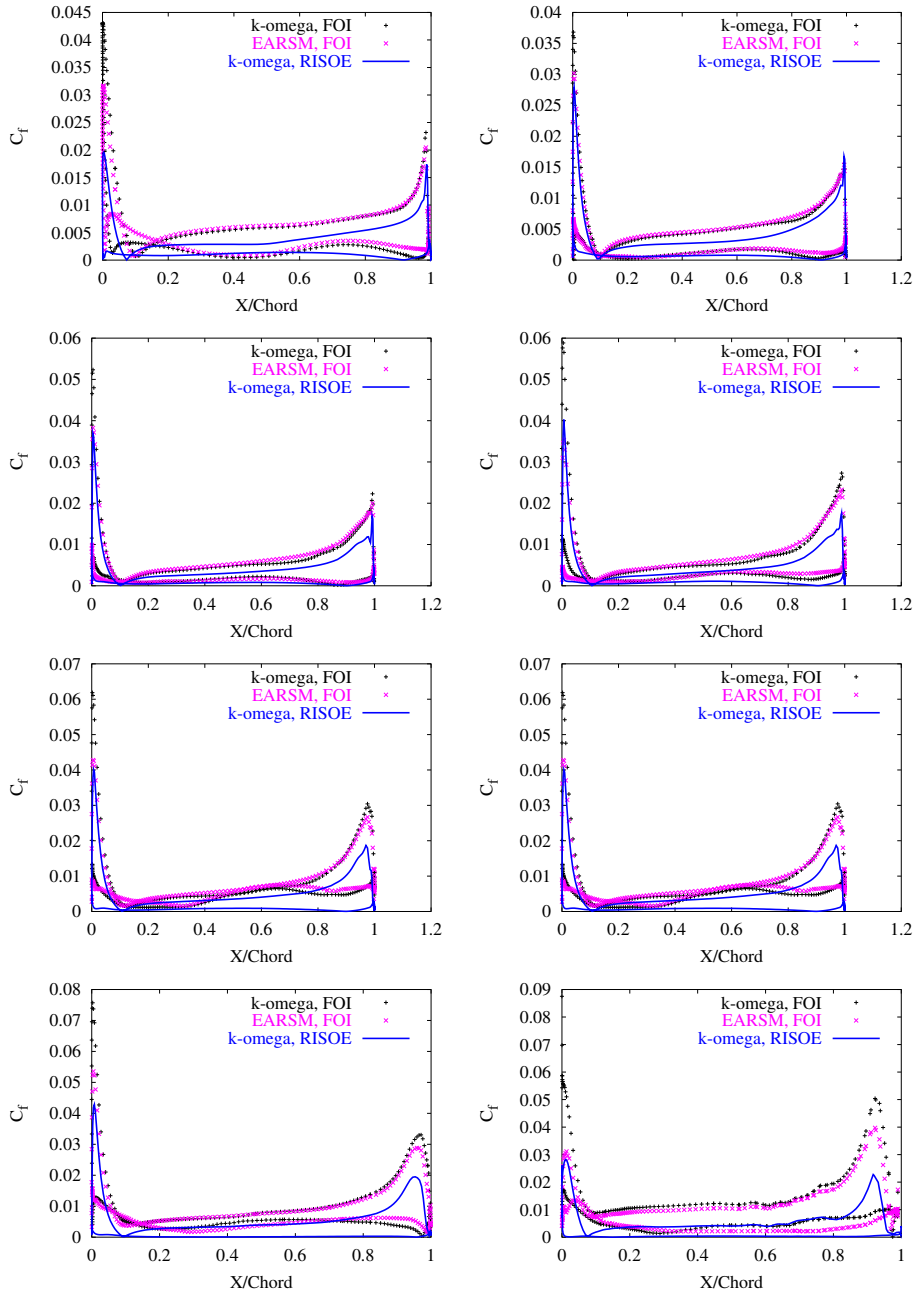

Figure 13. Comparison of the computed skin friction distributions for CASE-28.

Table 4. Flap and Edge-wise moment at r=0.432 [m] for the NREL PHASE-VI, CASE L2000ST0.

Component	EXP.	RISOE DES	RISOE RANS
Flap [Nm]	1615	1605	1617
Edge [Nm]	227	213	208

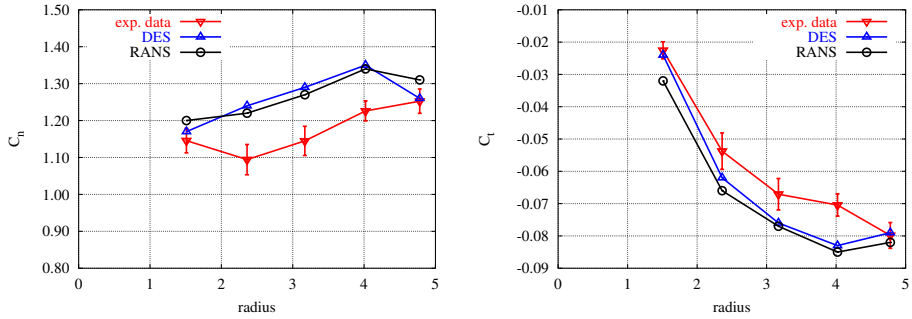

Figure 14. Spanwise distribution of normal and tangential force coefficients.

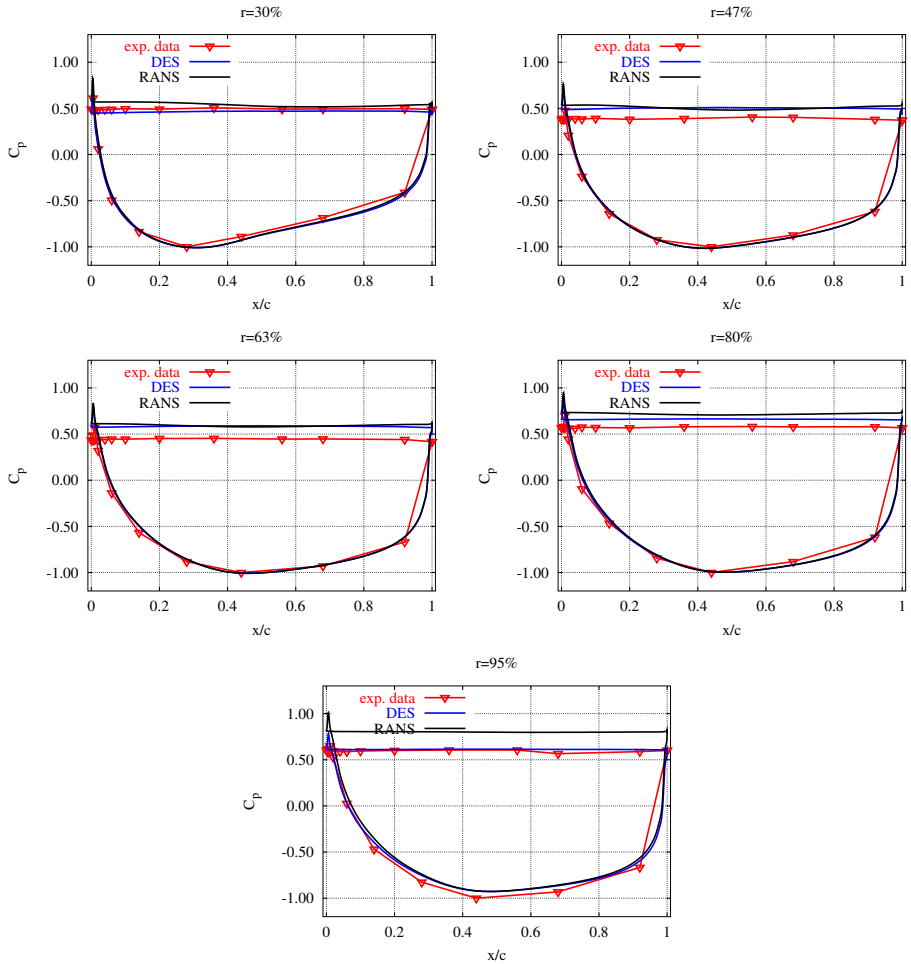

Figure 15. Pressure distributions at five spanwise positions along the NREL PHASE-VI blade.

Time series of the sectional normal and tangential force coefficients are shown in Figure 16. The most pronounced observation is the total lack of unsteadiness in the RANS simulation, where the simulation approaches a stationary value. Comparing the DES and the RANS simulation, the mean values of the simulations agree very well, which support previous findings that RANS simulations provide good predictions for the NREL PHASE-VI rotor. Comparing the simulated time series with measurements, the fact that the simulations and the measured signals are not correlated in time is obvious. Secondly, we find that there exists a high frequency content in the measured signal that is not predicted by the simulation. Finally, the offset observed previously for the mean values of the normal force is also observed here.

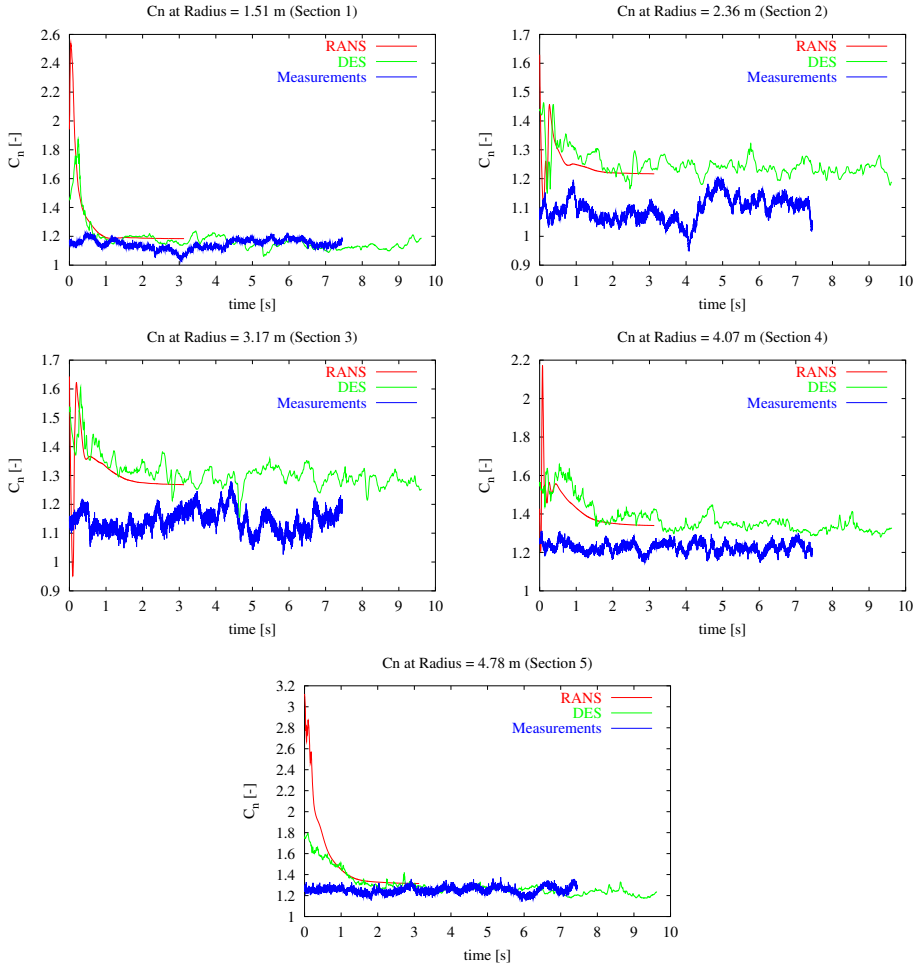

Figure 16. Time series of sectional normal forces.

Looking at the vortex pattern behind the rotor blade, there is a distinct difference between the RANS and DES wakes. Looking at Figur 17, showing a snapshot of the wake, the wake computed with the RANS model forms a few large-scale structures while the DES simulation predicts a variety of scales in the wake. There is no doubt that the DES simulation captures more of the real flow physics.

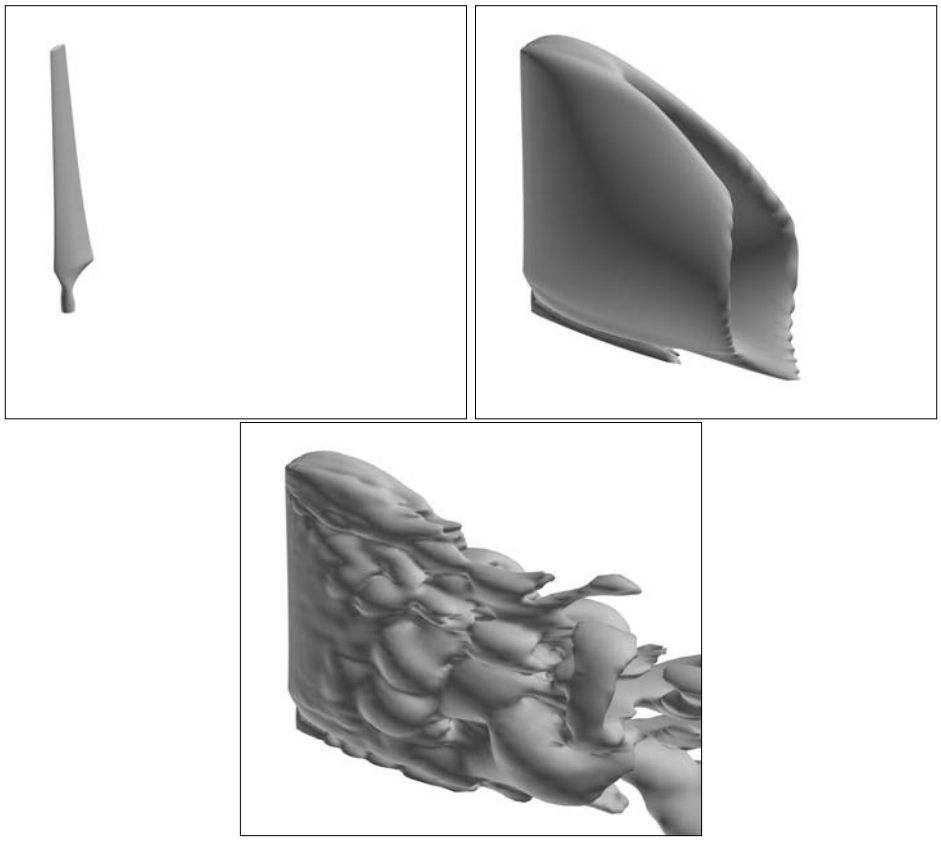

Figure 17. Wake pattern behind the parked NREL Phase-VI blade. The upper left figure shows the blade surface, the upper right figure shows the wake from the RANS simulation while the lower figure shows the wake from the DES simulation.

Overall performance of the NREL PHASE-VI computations

The difference between the time averaged values from the RANS and DES simulations are very minor. Only near the root and tip a consistent moderat improvement is found using DES. The deviation is for both types of turbulence models caused by an over-prediction of the suction on the lee side of the airfoil. From both the wake visualizations and the time traces of the normal force coefficients, the DES simulation shows an improved physical representation of the flow physics. Generally, both types of computations predict the forces on the blade within 20 percent along the total rotor blade.

5 Conclusion

Two rotors blades are computed during standstill conditions, the STORK 5.0 WPX blade and the NREL PHASE-VI blade. The STORK blade is computed at three different tip pitch angles, 0, 26 and 50, while the NREL blade is computed at 90 degrees tip pitch angle. Generally, the CFD codes reproduces the measured trends quite well and the two involved CFD codes, EDGE and EllipSys3D give very similar results. The deviations observed can be explained by the difference in the applied turbulence models and that the EDGE results are instantaneous values instead of averaged values. The comparison of steady and transient RANS results show, that with respect to mean quantities the gain of using time true computations is very limited for this case. The same can be said for the RANS/DES comparison performed for the NREL blade, even though the DES computation show improved agreement with measurments, at the tip and root sections. Finally, the DES methodology provides a much more physical representation of the heavily stalled part of the flow over blades at high angles of attack.

6 Acknowledgement

The work was carried out under a contract with EC, ENK6-CT-2001-00503, KNOW-BLADE. Computations by Risø were made possible by the use of the IBM RS6000 SP at the Risø central computing facility and the Danish Centre for Scientific Computing IBM SP90 facility in Århus.

References

[1] Brand A.J. and Montgomerie B. Quasi-Steady Aerodynamic Coefficients at a Large Range of Angles of Attack. Ecn-c-95-059, The Netherlands Energy Research Foundation (ECN), 1995.

[2] Montgomerie B. DRAG COEFFICIENT DISTRIBUTION ON A WING AT 90 DEGREES TO THE WIND. Ecn-c-95-061, The Netherlands Energy Research Foundation (ECN), 1996.

[3] A. Bjork, G. Ronsten, and B. Montgomerie. Aerodynamic Section Characteristics of a Rotating and Non-rotating 2.375 m Wind Turbine Blade. FFA TN 1995-03, FFA, Bromma, Sweden, 1995.

[4] Lindenburg C. Stall Coefficients, Aerodynamic Airfoil Coefficients at Large Angles of Attack. In *IEA Joint Action. Aerodynamics of wind turbines. 14th Symposium*, pages 133–148, Boulder, USA, December 2000.

[5] Ostawari C. and Naik D. Post Stall Studies of Untwisted Varying Aspect Ratio Blades with an NACA 4415 Airfoil Section - Part I. *Wind Engineering*, 8, No.3, 1984.

[6] Ostawari C. and Naik D. Post Stall Studies of Untwisted Varying Aspect Ratio Blades with an NACA 44XX Series Airfoil Section - Part II. *Wind Engineering*, 8, No.3, 1984.

[7] Wilcox D. C. A Half Century Historical Review of the K-ω Model. AIAA-91-0615, 1991.

[8] Simms D., Hand M.M., Fingersh L.J., and Jager D.W. Unsteady Aeorydnamics Experiment Phases II-IV: Test Configurations and Available Data Campaigns. NREL/TP -500-25950, Nat. Ren. Energy Lab., Golden, CO, 1999.

[9] Bertagnolio F., Sørensen N.N., Johansen J., and Fuglsang P. Wind Turbine Airfoil Catalogue. Risø-R- 1280-(EN), Risø National Laboratory, Roskilde, Denmark, 2001.

[10] Ronsten G. Static pressure measurements on a rotating and a non-rotating 2.375 m wind turbine blade. Comparison with 2D computations. *J. of Wind Engineering and Industrial Aerodynamics*, 39:105–118, 1992.

[11] Ronsten G. Geometry and Installation in Wind Tunnels of a STORK 5.0 WPX Wind Turbine Blade Equipped with Pressure Taps. Technical Report FFAP-A 1006, 1994.

[12] Issa R. I. Solution of the Implicitly Discretised Fluid Flow Equations by Operator-Splitting. *J. Computational Phys.*, 62:40–65, 1985.

[13] Issa R. I., Gosman A. D., and Watkins A. P. The Computation of Compressible and Incompressible Recirculating Flows by a Non-iterative Implicit Scheme. *J. Computational Phys.*, 62:66–82, 1986.

[14] Johansen J., Sørensen N.N., Michelsen J.A., and Schreck S. Detached-Eddy Simulation of Flow Around the S809 Airfoil. In *European Wind Energy Conference & Exhibition, Copenhagen, Denmark*, pages 414–417, 2-6 July 2001.

[15] Dahlberg J.-A. and Ronsten G. A Wind tunnel Investigation of Tower Blockage Effects and Parking Loads on a Œ 5.35 M Horizontal Axis Wind Turbine. In *5th European Wind Energy Association Conference and Exhibition, Copenhagen, Denmark*, volume II, pages 414–417, 10-14 October 1994.

[16] Michelsen J.A. Basis3D - a Platform for Development of Multiblock PDE Solvers. Technical Report AFM 92-05, Technical University of Denmark, 1992.

[17] Michelsen J.A. Block structured Multigrid solution of 2D and 3D elliptic PDE's. Technical Report AFM 94-06, Technical University of Denmark, 1994.

[18] Dekker J.W.M., de Groot C.M., and Spath M. Mechanical Measurements on VSH 20-WPX-THR Rotor Blades at the '25 HAWT' Rotor Test Facility - Part 1. Ecn-89-35, The Netherlands Energy Research Foundation (ECN), 1989.

[19] Khosla P. K. and Rubin S. G. A diagonally dominant second-order accurate implicit scheme. *Computers Fluids*, 2:207–209, 1974.

[20] Fingersh L., Simms D., Hand M., Jager D., Cortrell J., Robinsion M., Schreck S., and Larwood S. Wind Tunnel Testing of NREL's Unsteady Aeordynamics Experiment. In *2001 ASME Wind Energy Symposium*, pages 129–135, Reno, NV, January 11-14 2001. ASME. AIAA-2001-0035.

[21] Hand M., Simms D., Fingersh L.J., Jager D., and Larwood S. Cotrell J., Schreck S. Unsteady Aeorydnamics Experiment Phases VI: Wind tunnel Test Configurations and Available Data Campaigns. NREL/TP -500-29955, Nat. Ren. Energy Lab., Golden,CO, 2001.

[22] Strelets M. Detached Eddy Simulation of Massively Separated Flows. AIAA Paper 2001-0879, Russian Scientific Center "Applied Chemistry" St. Petersburg, 2001.

[23] Sørensen N. N. General Purpose Flow Solver Applied to Flow over Hills. Risø-R- 827-(EN), Risø National Laboratory, Roskilde, Denmark, June 1995.

[24] Sørensen N.N. and Michelsen J.A. Drag Prediction for Blades at High Angle of Attack Using CFD. AIAA Paper 2004-0831, 2004.

[25] Eliason P. EDGE, a Navier-Stokes solver for unstructured grids. Technical Report FOI-R–0298–SE, 2002.

[26] Giguere P. and Selig M.S. Design of a Tapered and Twisted Blade for the NREL Combined Experiment Rotor. NREL/SR -500-26173, Nat. Ren. Energy Lab, Golden, CO, April 1999.

[27] U.S. Paulsen. Aerodynamics of full Scale, Non Rotating Wind turbine Blade Under Natural Wind Conditions. Risø-M- 2768, Risø National Laboratory, Roskilde, Denmark, 1989.

[28] Menter F. R. Zonal Two Equation k-ω Turbulence Models for Aerodynamic Flows. AIAA-paper-932906, 1993.

[29] Wallin S. and Johansson A. A complete explicit Algebraic Reynolds Stress Model for Incompressible and Compressible Turbulent Flows. *JFM*, (403):89–132, 2000.

[30] Yang S.L., Chang Y.L., and Arici O. Navier-Stokes Computations of the NREL Airfoil Using a $k-\omega$ Turbulent Model at High Angles of Attack. *J. Solar Energy*, 117:304–310, 1995.

Bibliographic Data Sheet **Risø-R-1465(EN)**

Title and author(s)

CFD Computations of Wind Turbine Blade Loads During Standstill Operation
KNOW-BLADE, TASK 3.1 Report

Niels N. Sørensen, Jeppe Johansen, Stephen Conway

Abstract (Max. 2000 char.)

Two rotors blades are computed during standstill conditions, using two different Navier-Stokes solvers EDGE and EllipSys3D. Both steady and transient linear $k-\omega$ RANS turbulence models are applied, along with steady non-linear RANS and transient DES simulations. The STORK 5.0 WPX blade is computed a three different tip pitch angles, 0, 26 and 50 degrees tip pitch angle, while the NREL Phase-VI blade is computed at 90 degrees tip pitch angle. Generally the CFD codes reproduce the measured trends quite well and the two involved CFD codes give very similar results. The discrepancies observed can be explained by the difference in the applied turbulence models and the fact that the results from one of the solvers are presented as instantaneous values instead of averaged values. The comparison of steady and transient RANS results show that the gain of using time true computations are very limited for this case, with respect to mean quantities. The same can be said for the RANS/DES comparison performed for the NREL rotor, even though the DES computation shows improved agreement at the tip and root sections. Finally, it is shown that the DES methodology provides a much more physical representation of the heavily stalled part of the flow over blades at high angles of attack.

ISBN
87-550-3343-1(Internet)

ISSN
0106-2840

Dept. or group
Risø National Laboratory
Wind Energy Department

Date
June 2004

Groups own reg. number(s)

Project/contract No.
1110033-00

Pages	Tables	Illustrations	References
27	2	17	30

Descriptors INIS/EDB

AERODYNAMICS; AIRFOILS; COMPUTATIONAL FLUID DYNAMICS; FLOW MODELS; NAVIER-STOKES EQUATIONS; THREE-DIMENSIONAL CALCULATIONS; TURBINE BLADES; TURBULENT FLOW; WIND TURBINES